Supporting Information

All-Inkjet-Printed Flexible Nanobio-Devices with Efficient Electrochemical Coupling Using Amphiphilic Biomaterials

Tae-Hyung Kang[†§], Seung-Woo Lee[‡], Kyowook Hwang[‡], Wonbo Shim[§], Ki-Young Lee[†], Jung-Ah Lim[†], Woong-Ryeol Yu[§], In-Suk Choi[*§], and Hyunjung Yi[*†]*

† Post-Silicon Semiconductor Institute, Korea Institute of Science and Technology, Seoul, 02792, Republic of Korea

‡ Department of Fine Chemistry, Seoul National University of Science and Technology, Seoul, 01811, Republic of Korea

§ Department of Materials Science and Engineering, Seoul National University, Seoul, 08826, Republic of Korea

E-mail: hjungyi@kist.re.kr, insukchoi@snu.ac.kr, woongryu@snu.ac.kr.

T.-H.K. and S.-W.L. contributed equally to this work.

Includes one supplementary method, 25 supplementary figures, one supplementary table, and one supplementary reference.

Supplementary Method

1) A detailed description of the numerical simulation

Numerical simulation was performed to determine the processing parameters under which the solution formed a single drop. Comsol Multiphysics was used to simulate the jetting behavior of the nanobio-ink of SWNTs and M13 phage (10:1). The simulations were based on a structured Eulerian grid, a finite element discretization and a level-set method.

The velocities of ink and air are much smaller than the speed of sound, so they can be considered incompressible. The incompressible Navier-Stokes equation describes the transport of mass and momentum. The Navier-Stokes equations are followed:

$$\rho \left(\frac{\partial \boldsymbol{u}}{\partial t} + \boldsymbol{u} \cdot \nabla \boldsymbol{u} \right) - \nabla \left(\mu (\nabla \boldsymbol{u} + \nabla \boldsymbol{u}^T) \right) + \nabla p = \boldsymbol{F}_{st}$$

$$(\nabla \cdot \boldsymbol{u}) = 0$$

where ρ is the density (kg m^{-3}), μ is the dynamic viscosity (N s m^{-2}), $\boldsymbol{u}$ represents the velocity (m s^{-1}), p denotes pressure (Pa), and $\mathbf{F}_{st}$ is the surface tension force.

The viscosity of the fluid was implemented by fitting the data shown in Figure S2a to the carreau model.

A simple axis symmetry model of the nozzle was used, as shown in Figure S3. The following boundary conditions were used. A no-slip wall boundary was applied at the right boundary, as shown by the blue lines in Figure S3b. A velocity boundary was imposed where the inlet boundary, as shown by the blue lines in Figure S3c. This boundary can be expressed as follows:

$$\boldsymbol{u} = -U_0 \boldsymbol{n}$$

$$U_0 = a \times v_t \times v_r$$

$$v_t = \left(\text{step}(t) - \text{step}(t - t_1)\right)$$

$$v_r = \left(\frac{r + 0.08}{0.16}\right) \times \left(1 - \frac{r + 0.08}{0.16}\right)$$

where v_r denotes the radial dependent inlet velocity, v_t is the time-dependent inlet velocity, and step(t) is a smooth step function. a and t_1 are variables for processing parameters (see Figure S3e).

A pressure boundary was imposed at the outlet boundary. The pressure at this boundary was $p = p_{ref} + p_0 = p_{ref} = 1$. This boundary can be expressed as:

$$[-p\boldsymbol{I} + \mu(\nabla \boldsymbol{u} + (\nabla \boldsymbol{u})^T)]\boldsymbol{n} = -\hat{p}_0 \boldsymbol{n}$$

$$\hat{p}_0 \leq p_0$$

Supplementary Figures
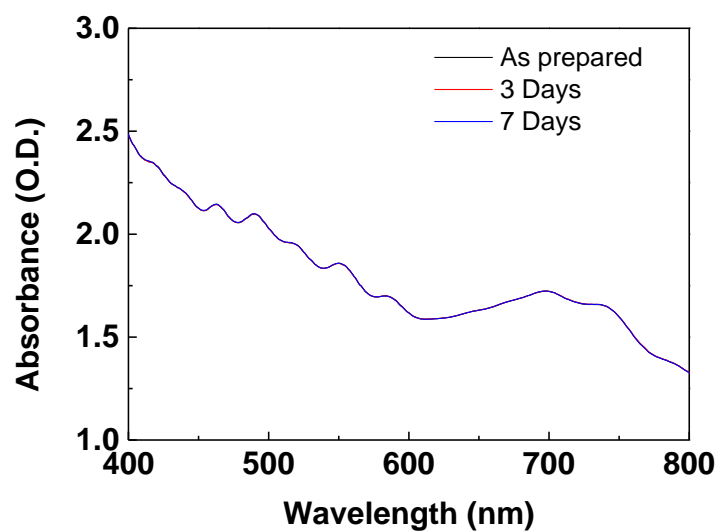
Figure S1. Comparison of the absorption curve of the as-prepared nanobio-ink (SWNT/M13 = 10:1) with those measured after storing three and seven days.
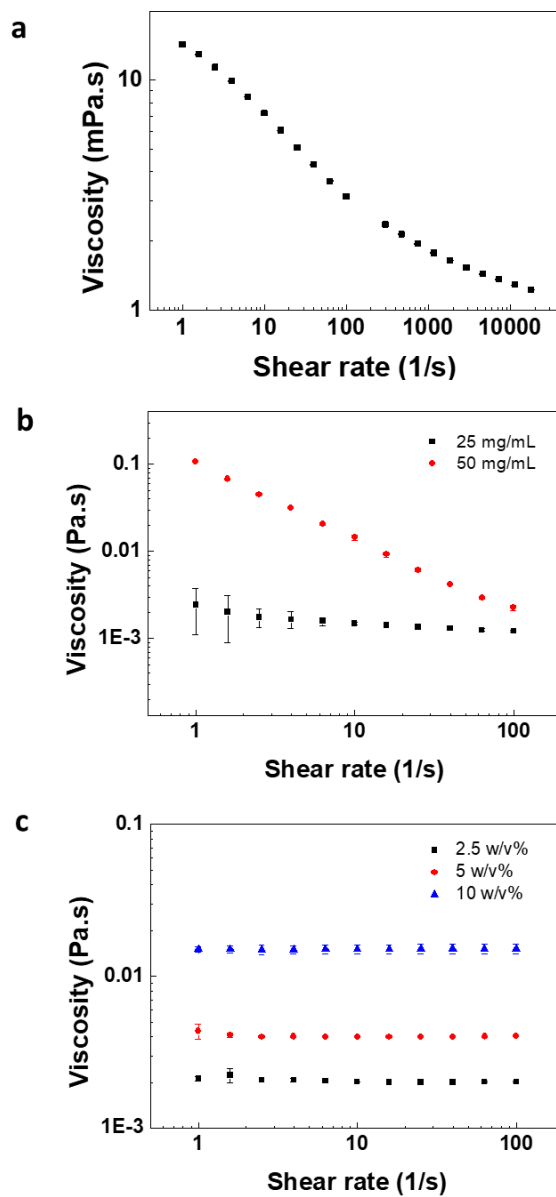
Figure S2. Physical properties of formulated inks. (a-c) Changes in dynamic viscosity at 25°C for (a) SWNT–M13 phage solution (10:1) with broad shear rates for fitting to carreau model, (b) GOx aqueous solution in 10 mM PBS and (c) PEI aqueous solution. Mean values ± SD were obtained from three different samples.
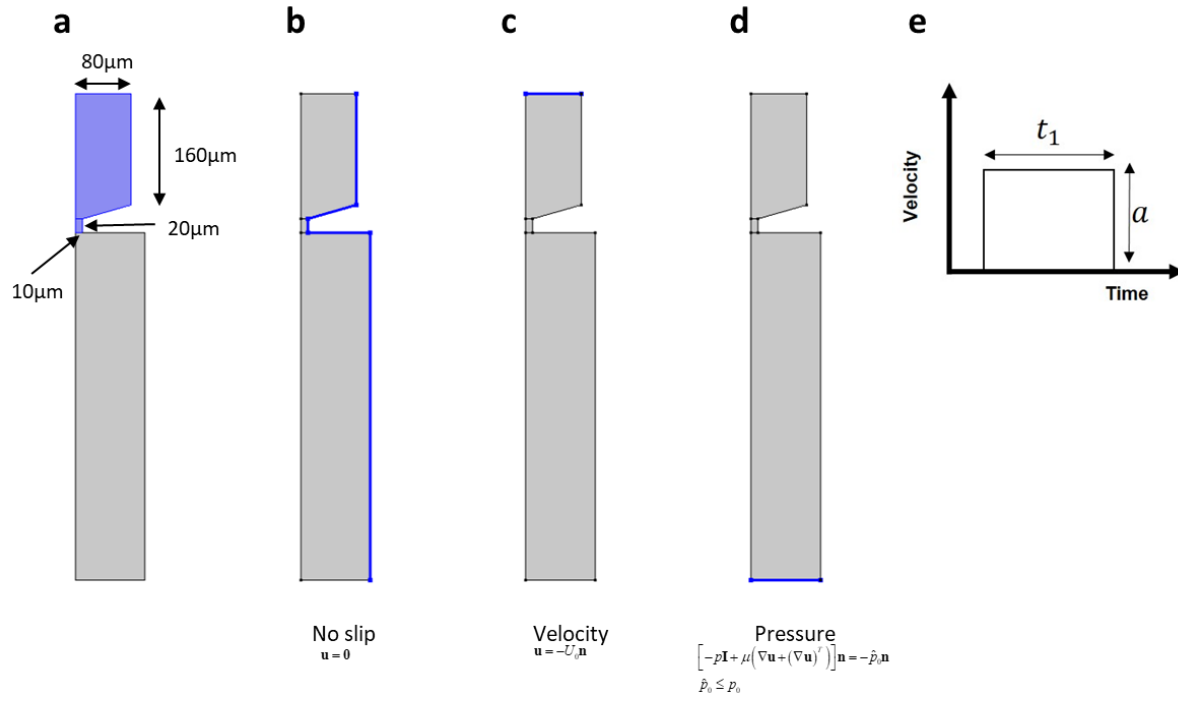
Figure S3. Axis symmetry geometry and boundary conditions of the modeled nozzle: (a) The details of geometry, (b) no-slip boundary, (c) velocity boundary in inlet, (d) pressure boundary in outlet, and (e) Parameters for inlet boundary conditions. a is inlet velocity and t_1 is the time of injection.
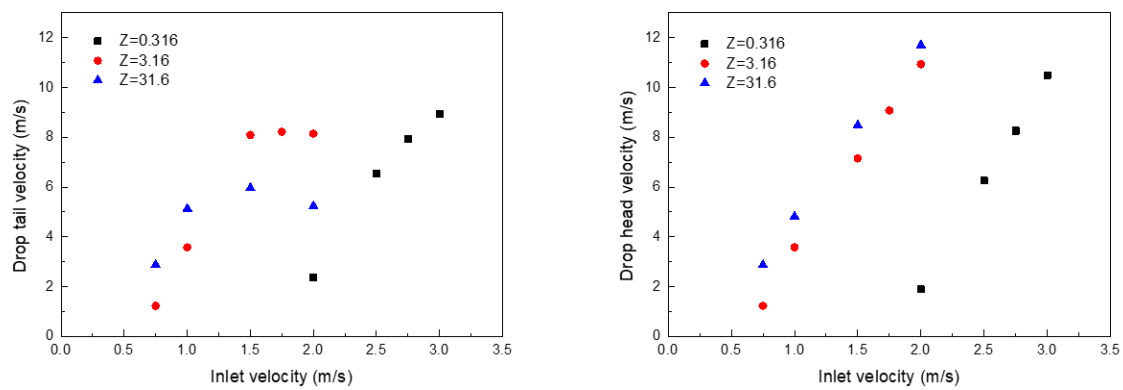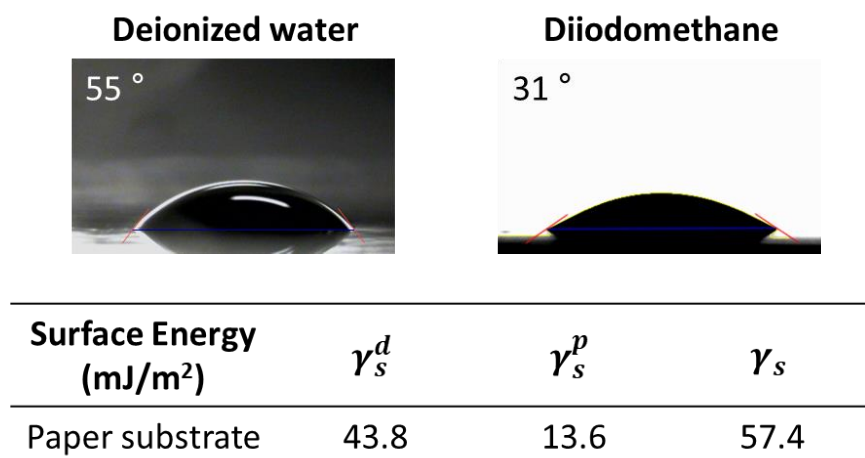
Figure S4. Dependence of the simulated drop tail and head velocities for ink solutions of different Z values on the inlet velocity.
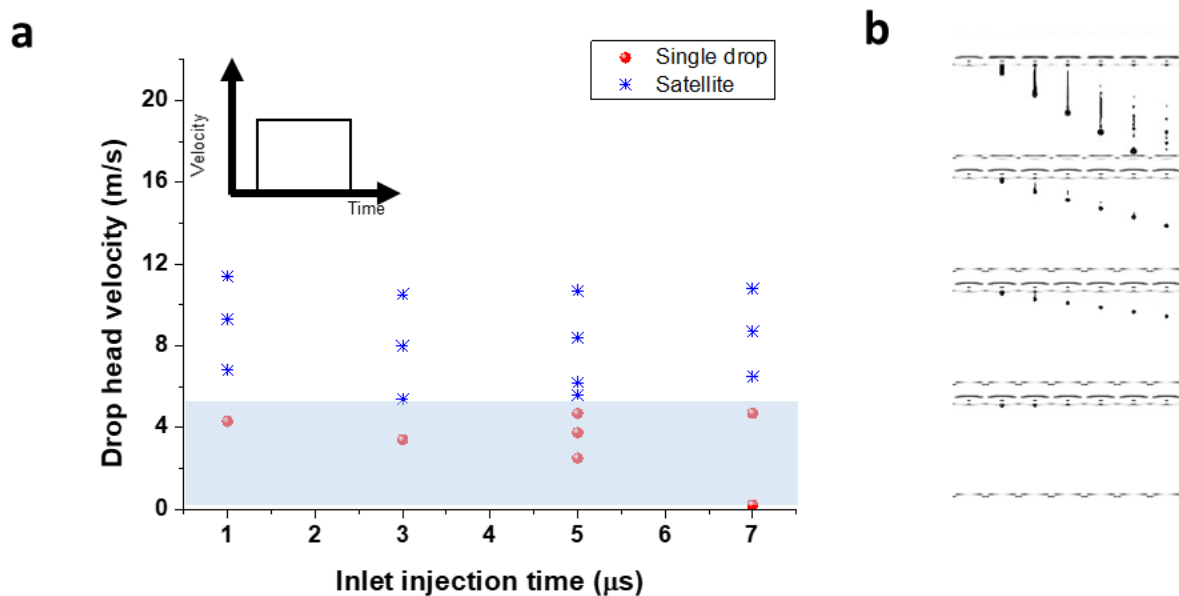
Figure S5. Numerical simulation results for drop head velocity jetted at various conditions. (a) Drop head velocity values jetted at various conditions. The calculation suggested that the drop head velocity seemed to be highly related to the formation of a single drop: when the drop head velocity was about 5 m s^{-1} or lower, a single drop successfully formed. (b) Images of typical four different types of simulated jetting behavior, satellite drop formation, single drop formation with tail retraction, single drop formation, and non-jetting, from the top row.

Deionized water	Diiodomethane
55 °	31 °

Surface Energy (mJ/m²)	γ_s^d	γ_s^p	γ_s
Paper substrate	43.8	13.6	57.4

Figure S6. Contact angles of deionized water and diiodomethane on the paper substrate used in this study. The surface energy was calculated based on the Owens-Wendt method.[S1]

γ_s^d: Dispersive component of surface energy

γ_s^p: Polar component of surface energy
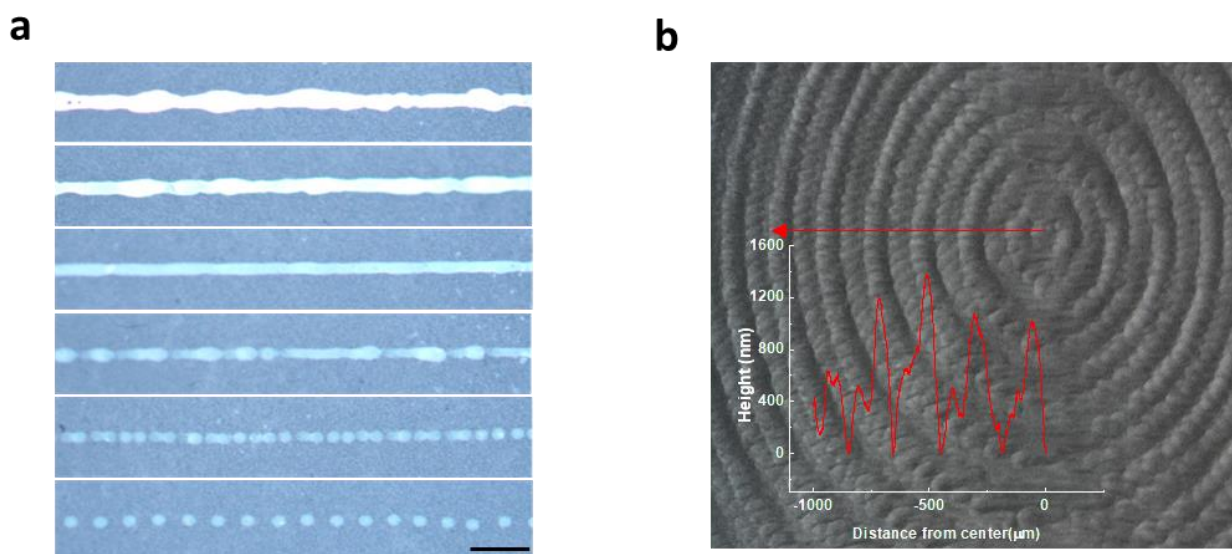
Figure S7. Effect of drop spacing on morphologies of printed nanobio-inks on a glossy paper. (a) Various morphologies printed at various drop spacing values, 5, 10, 20, 30, 40 and 100 μm from the top to the bottom rows. Scale bar: 200 μm (b) Optical micrograph of printed concentric circles at an interval of 100 μm. Inset: Height profiles of the printed concentric circles.
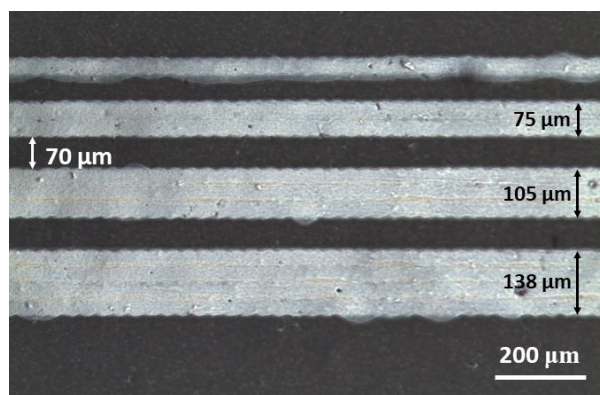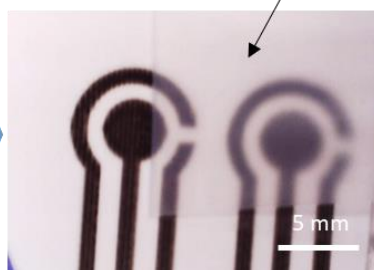
Figure S8. Optical micrograph of inkjet-printed lines with various widths. The minimum feature size is about 75 μm and the minimum spacing is about 70 μm.
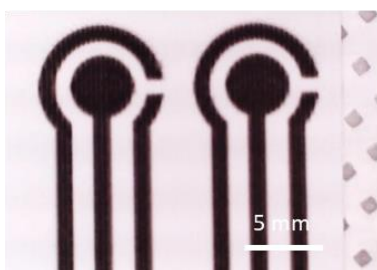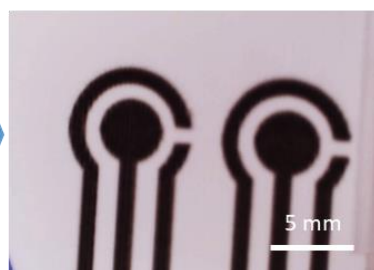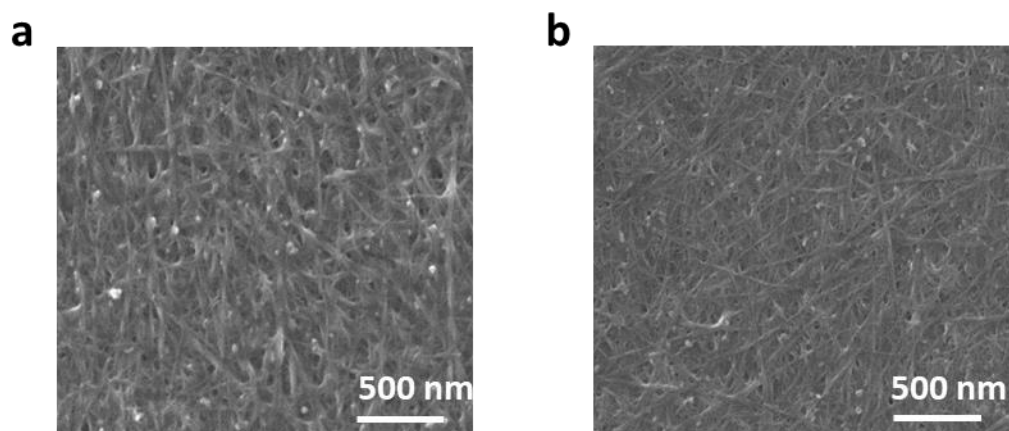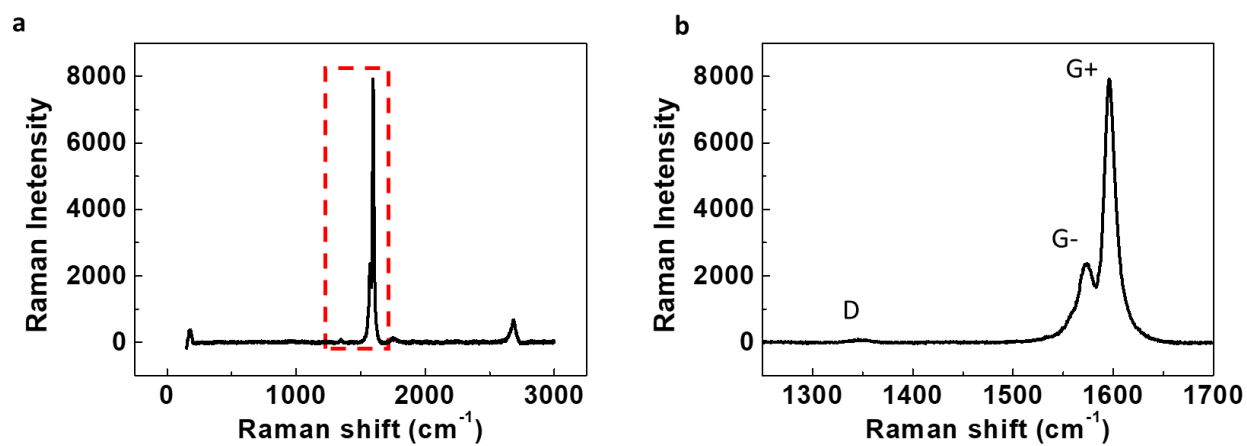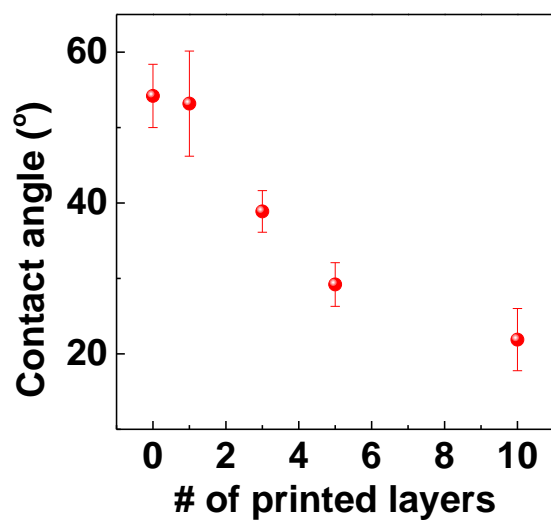
Figure S9. Photographs of the inkjet-printed electrode showing its stable adhesion with the paper substrate.

Figure S10. Scanning electron micrographs of the (a) as-printed and (b) washed nanobio-electrodes.

Figure S11. (a) Full range Raman spectrum of the inkjet-printed SWNT–M13 electrode. (b) Detailed Raman spectrum shown in the red dotted box in (a).
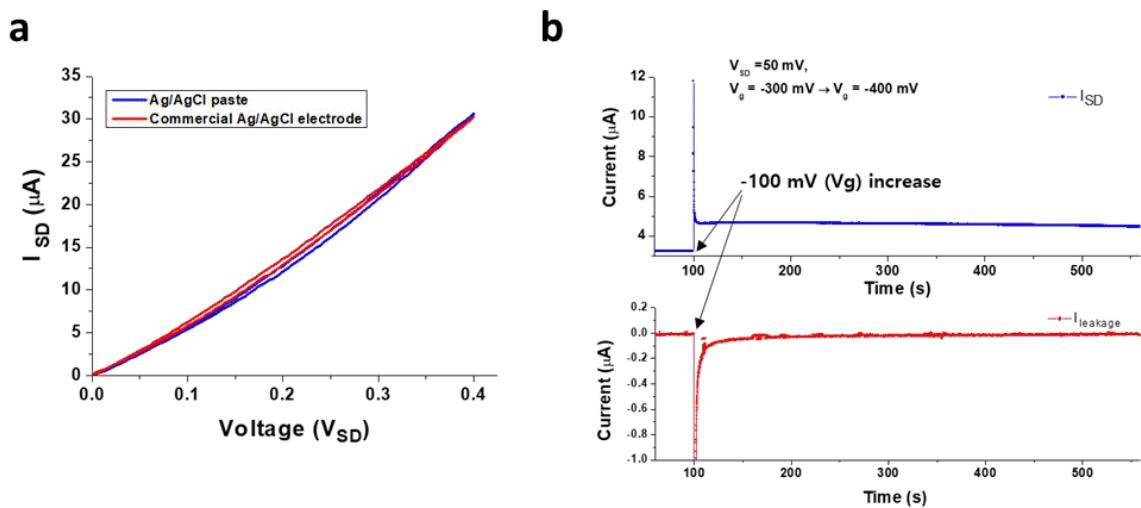
Figure S12. Dependence of the contact angle of the SWNT–M13 electrode on the number of print. The molar ratio of SWNT/M13 phage = 10:1. Mean values ± SD were obtained from three different samples.
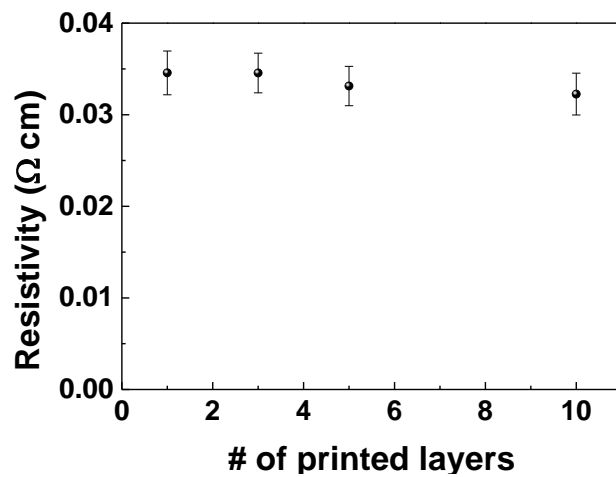
Figure S13. Dependence of the resistivity on the number of print. The molar ratio of SWNT/M13 phage = 10:1. Mean values ± SD were obtained from five different samples.
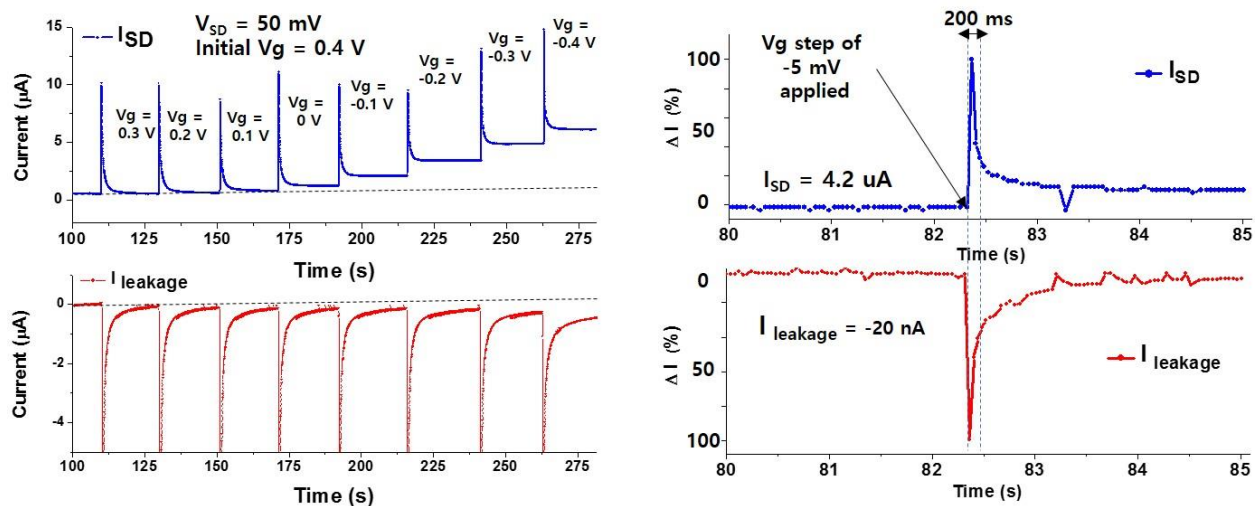
Figure S14. (a) Comparison of the printed gate electrode coated with Ag/AgCl paste and the commercial Ag/AgCl electrode. (b) Stable operation of the printed gate electrode coated with Ag/AgCl paste of the all-inkjet-printed eFET.
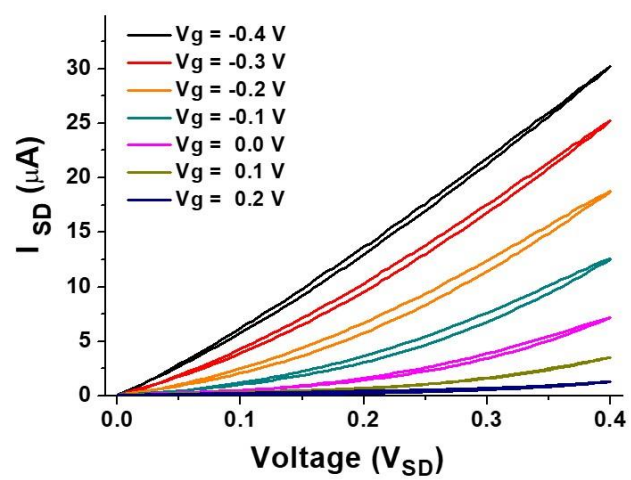
**Figure S15**. Output curves of the all-inkjet-printed eFET.

Figure S16. (a) Channel and leakage current levels measured by increasing the gate potential stepwise. (b) Channel and leakage current levels measured by applying gate potential of -5 mV step. The time constant of 200 ms was estimated from the time point when the current by the double-layer capacitance dropped to 37% of the initial value upon the -5 mV step of the gate potential.
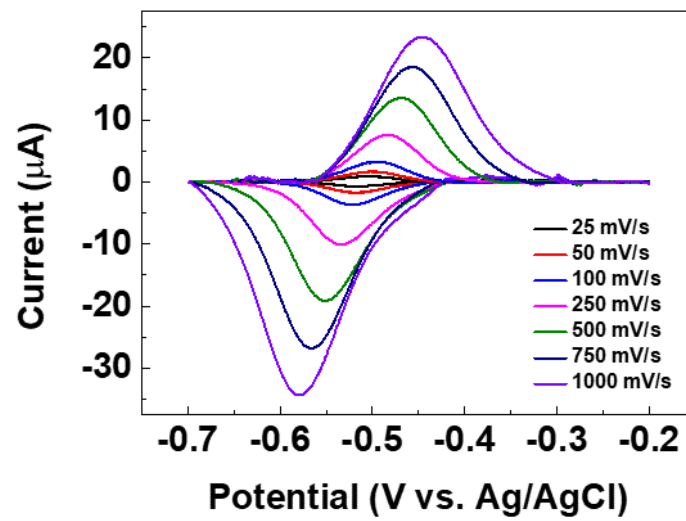
Figure S17. CV curves after subtraction of background capacitive currents of Figure 3e.
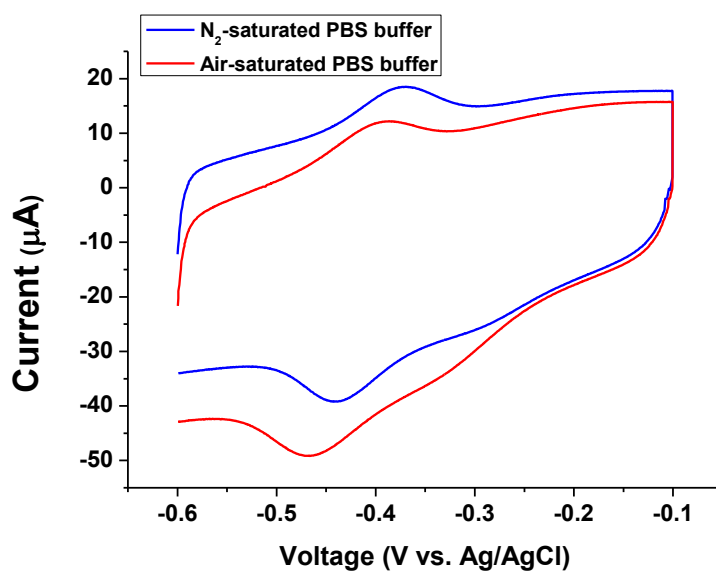
Figure S18. Effect of the buffer condition on the all-printed electrode in N_2-saturated 10 mM PBS buffer and air-saturated 10 mM PBS buffer. Compared to the N_2-saturated buffer environment (blue curve), the reduction current increased in the air-saturated buffer (red curve) since oxygen in the electrolyte regenerated GOx (FAD) from GOx (FADH$_2$).
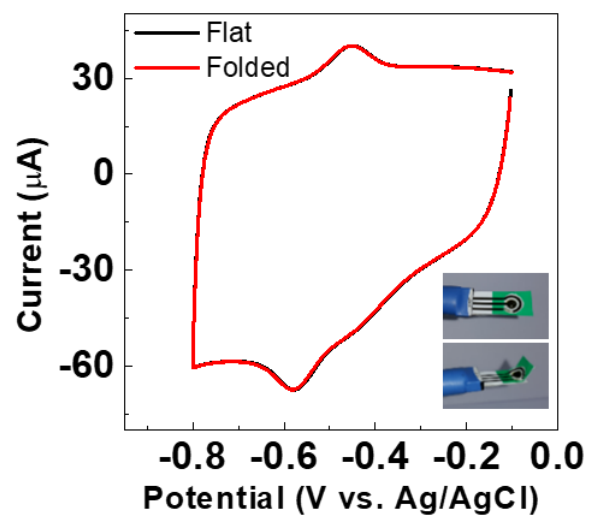
Figure S19. CV curves measured from the paper-based biosensor before and after folding by 90°. Inset: Photographs showing the tested biosensors.
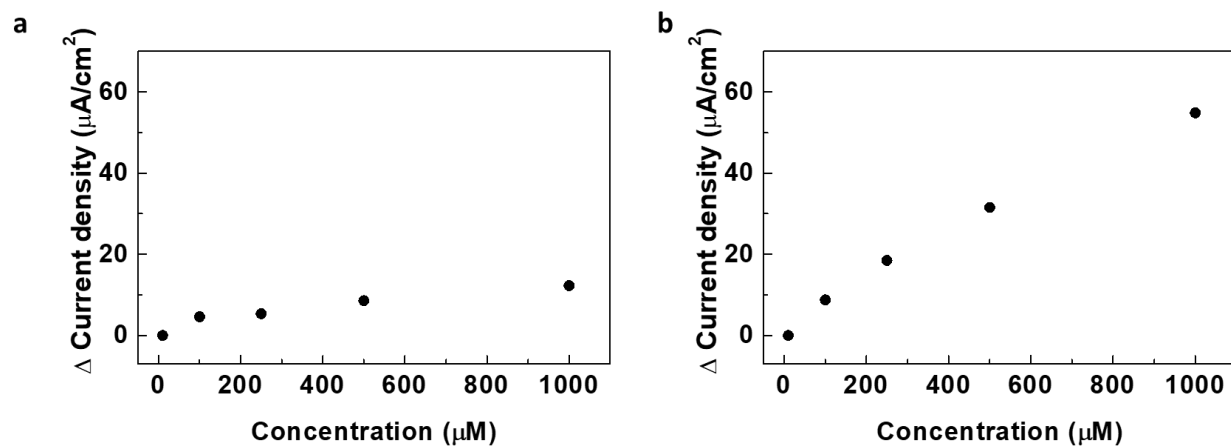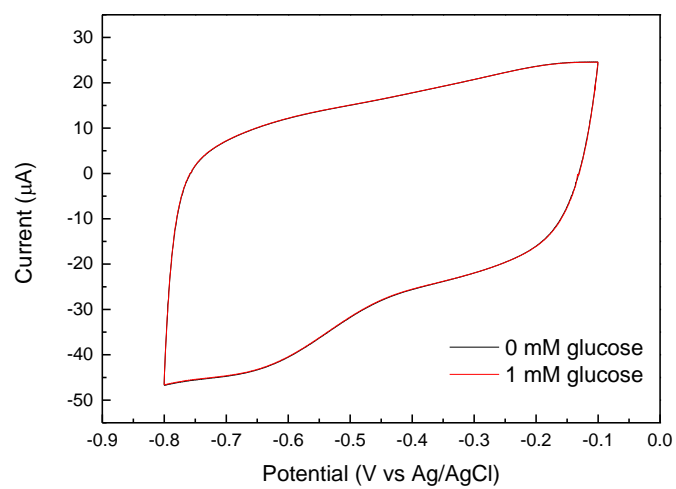
Figure S20. The changes in the cathodic peak current density with increasing glucose concentration of the inkjet-printed electrode with (a) six and (b) ten layers of GOx ink solution.
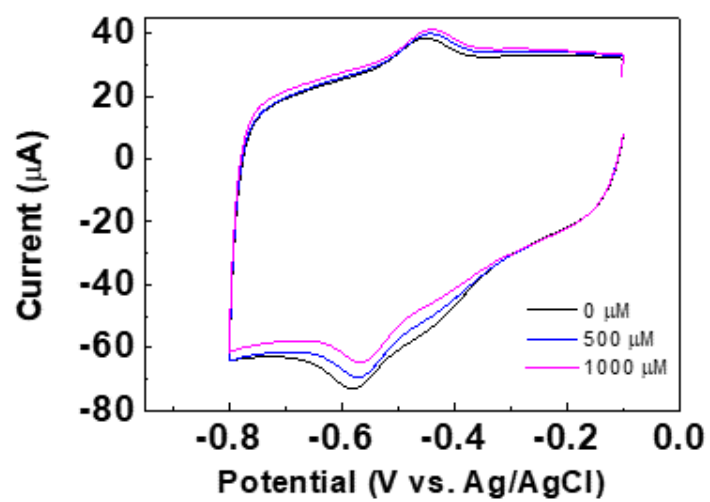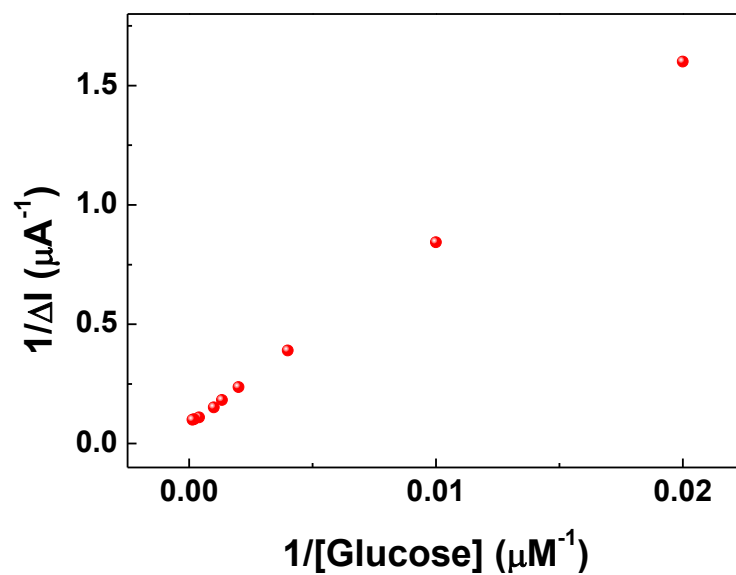
Figure S21. CV curves of the all-inkjet-printed enzymatic biosensors measured in buffer solutions containing various glucose concentrations.
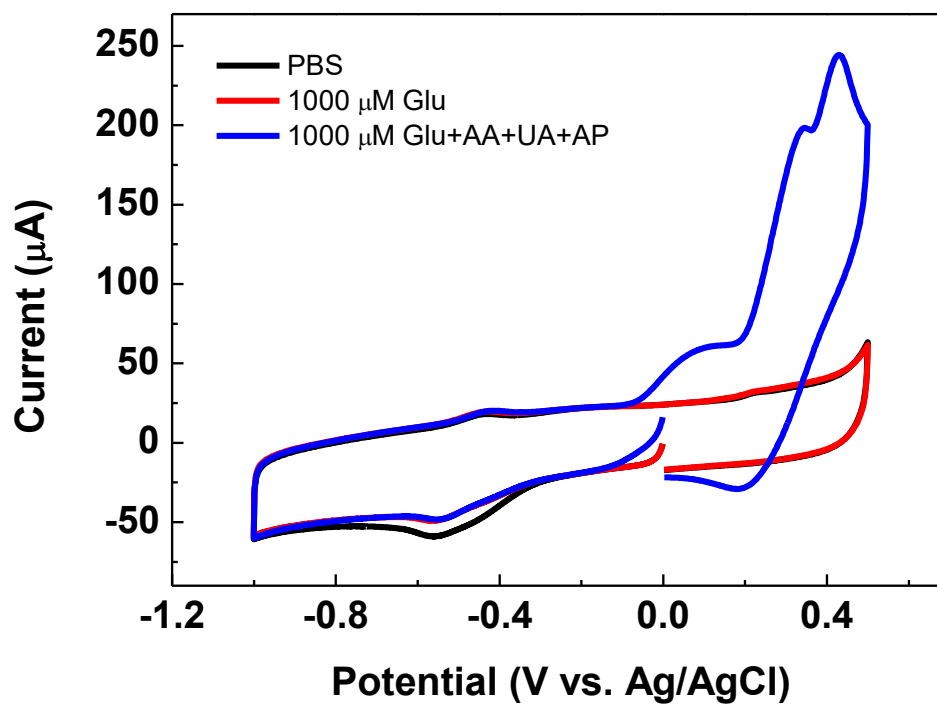
Figure S22. CV curves of the SWNT–M13 only electrode without GOx measured in PBS with 0 mM and 1 mM glucose concentrations.

Figure S23. Lineweaver-Burk plot for catalyzed glucose electro-oxidation on the SWNT–M13-PEI-GOx sensor.

.

Figure S24. High selectivity of the all-inkjet-printed glucose sensors. The addition of 1 mM of interfering materials such as ascorbic acid (AA), acetaminophen (AP), and uric acid (UA) did not significantly alter the DET peaks of GOx.
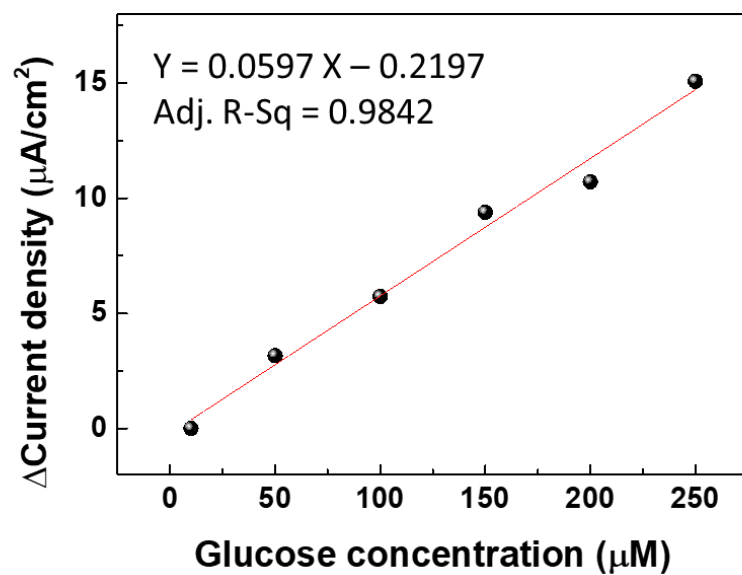
Figure S25. Calibration curve of the all-inkjet-printed glucose biosensor used for calculating the sweat glucose level.

Table S1. Parameters used for inkjet-printing of all the functional inks used in the study.

			SWNT–M13 solution	PEI solution	GOx solution
Firing voltage (V)			30-35	15-20	25-30
Jetting frequency (kHz)			2	2	2
Jetting segment 1		Level (%)	100	100	
		slew rate	0.2	0.3	
		Duration (µs)	9.984	5.632	
Jetting segment 2		Level (%)	0	0	
		slew rate	0.1	0.06	
		Duration (µs)	14.976	21.248	
Non-jetting segment 1		Level (%)	13	27	
		slew rate	1	0.3	
		Duration (µs)	6.528	5.632	
Non-jetting segment 2		Level (%)	0	0	
		slew rate	1	0.06	
		Duration (µs)	18.432	21.248	
Cleaning			Spit cleaning every 240 bands	Manual cleaning after printing each layer	

Supplementary reference

(1) Kim, S. J.; Jang, M.; Yang, H. Y.; Cho, J.; Lim, H. S.; Yang, H.; Lim, J. A. Instantaneous Pulsed-Light Cross-Linking of a Polymer Gate Dielectric for Flexible Organic Thin-Film Transistors. *ACS Appl. Mater. Interfaces* **2017**, 9 (13), 11721-11731